Efficiently unquenching QCD+QED at $O(\alpha)$

Tim Harris,[a,*] **Vera Gülpers,**[a] **Antonin Portelli**[a] **and James Richings**[a,b]

[a] *School of Physics and Astronomy, University of Edinburgh,*
Edinburgh EH9 3FD, United Kingdom

[b] *EPCC, University of Edinburgh,*
EH8 9BT, Edinburgh, United Kingdom

E-mail: tharris@ed.ac.uk

We outline a strategy to efficiently include the electromagnetic interactions of the sea quarks in QCD+QED. When computing iso-spin breaking corrections to hadronic quantities at leading order in the electromagnetic coupling, the sea-quark charges result in quark-line disconnected diagrams which are challenging to compute precisely. An analysis of the variance of stochastic estimators for the relevant traces of quark propagators helps us to improve the situation for certain flavour combinations and space-time decompositions. We present preliminary numerical results for the variances of the corresponding contributions using an ensemble of $N_\mathrm{f} = 2+1$ domain-wall fermions generated by the RBC/UKQCD collaboration.

The 39th International Symposium on Lattice Field Theory (Lattice2022),
8-13 August, 2022
Bonn, Germany

---

[*]Speaker

1. Introduction

Several lattice QCD predictions which form important input for precision tests of the Standard Model have uncertainties at or below the 1% level, for example the HVP contribution to $(g - 2)_\mu$, f_K/f_π, g_A or the Wilson flow scale $\sqrt{t_0}$ to name a few [1, 2]. However, to further improve such predictions, QCD with iso-spin symmetry is not a sufficiently accurate effective description of the low-energy dynamics and QED, which contributes one source of iso-spin breaking due to the different up- and down-quark electric charges, must be included. Recent efforts have been successful at including iso-spin breaking corrections, and some of which fully account for the effects of the sea-quark electric charges [3, 4, 5, 6, 7]. Nevertheless, many computations of iso-spin breaking effects still neglect to incorporate these dynamical effects in an approximation known as electroquenching. As the FLAG report notes in Section 3.1.2 [2], computations using the electroquenched approximation might feature an uncontrolled systematic error.

In this work we aim to include the effects of the electric charge of the sea quarks in the perturbative method known as the RM123 approach. This amounts to computing at least two additional Wick contractions. In order to sum the vertices in the resulting diagrams over the lattice volume, some approximations must be used which often introduce additional fluctuations, for example due to the auxiliary fields of a stochastic estimator. Here we investigate some simple decompositions which may avoid large contributions to the variance, so that sufficiently precise results can be obtained to systematically include all sources of iso-spin breaking without incurring a large computational cost.

2. Sea-quark effects in the RM123 method

Due to the smallness of the fine-structure constant $\alpha \sim 1/137$ and the renormalized light-quark mass difference $(m_u^R - m_d^R)/\Lambda \sim 1\%$, it is natural to expand physical observables (i.e. in QCD+QED) in these parameters to compute iso-spin breaking corrections, as was first outlined in Refs. [8, 9]. In the resulting expansion of an observable O

$$\langle O \rangle = \langle O \rangle \Big|_{e=0} + \tfrac{1}{2}e^2 \Big[\frac{\partial}{\partial e} \frac{\partial}{\partial e} \langle O \rangle \Big]_{e=0} + \dots \tag{1}$$

the leading corrections in the electric charge $e = \sqrt{4\pi\alpha}$ are parameterized in terms of the correlation function

$$\frac{\partial}{\partial e} \frac{\partial}{\partial e} \langle O \rangle = (-i)^2 \int d^4x \int d^4y \, \langle J_\mu(x) A_\mu(x) J_\nu(y) A_\nu(y) O \rangle_c \tag{2}$$

where the electromagnetic current for u, d, s quark flavours is defined

$$J_\mu = \sum_{f=u,d,s} Q_f \bar\psi_f \gamma_\mu \psi_f, \qquad Q_u = \tfrac{2}{3}, \quad Q_d = Q_s = -\tfrac{1}{3}. \tag{3}$$

By choosing the expansion point to be a theory with $\alpha = 0$ and iso-spin symmetry $m_u = m_d$, only correlation functions in the $N_f = 2 + 1$ theory need to be evaluated, which we denote with $e = 0$ in Eq. (1). The precise definition of such a theory using an additional set of renormalization conditions is necessary to fix the meaning of the leading-order term on the right-hand side (and
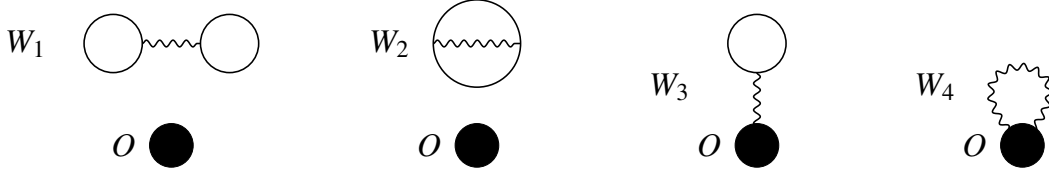
Figure 1: Wick contractions which appear at leading order in the expansion of a hadronic observable O in the electromagnetic coupling. Each closed fermion line has contributions from all of the quark flavours u, d, s, ... with the appropriate charge factors.

conversely the iso-spin breaking corrections themselves). Otherwise the predictions of QCD+QED are unambiguously defined, up to its intrinsic accuracy, by fixing N_f quark masses and the QCD coupling as the electric coupling does not renormalize at this order. In the above, the ellipsis stands for the mass counterterms which are needed to make physical predictions due to the contribution to the quark self-energy induced by QED.

After integrating out the fermion and photon fields, the resulting Wick contractions W_i are shown in Fig. 1, which contribute to the derivative with respect to the electric charge through the connected correlation function

$$\frac{\partial}{\partial e}\frac{\partial}{\partial e}\langle O\rangle = \sum_{i=1}^{4}\langle OW_i\rangle_{\mathrm{c}}. \tag{4}$$

The first two subdiagrams, which arise soley from the electric charges of the sea quarks, can be expressed in terms of a convolution with the photon propagator (in some fixed gauge) $G_{\mu\nu}(x) = \langle A_\mu(x)A_\nu(0)\rangle$

$$W_{1,2} = -a^8 \sum_{x,y} H_{1,2}^{\mu\nu}(x,y)G_{\mu\nu}(x-y), \tag{5}$$

where $H_{1,2}$ are the traces of quark propagators $S_f(x,y) = \langle \psi_f(x)\bar{\psi}_f(y)\rangle$

$$H_1^{\mu\nu}(x,y) = \sum_{f,g} Q_f Q_g \operatorname{tr}\{\gamma_\mu S_f(x,x)\} \operatorname{tr}\{\gamma_\nu S_g(y,y)\}, \tag{6}$$

$$H_2^{\mu\nu}(x,y) = -\sum_{f} Q_f^2 \operatorname{tr}\{\gamma_\mu S_f(x,y)\gamma_\nu S_f(y,x)\}. \tag{7}$$

These two diagrams are the main subject of these proceedings, and the techniques advocated for the first can be effectively reused for the third diagram, W_3. In the following sections we introduce stochastic estimators only for the quark lines and compute the subdiagrams by convoluting with the exact photon propagator which avoids introducing additional stochastic fields for the U(1) gauge potential. The final diagram W_4, which only contributes if the observable O depends explicitly on the (charged) fermion fields, is the only one surviving the electroquenched approximation, and, can in most cases be computed efficiently provided that the leading-order diagram is already under control.

We note that the variance of the contributions to the connected correlation functions on the r.h.s. of Eq. (4) crudely factorizes

$$\sigma^2_{OW_{1,2}} \approx \langle O \rangle^2_c \langle W_{1,2} \rangle^2_c + \langle OW_{1,2} \rangle^2_c \tag{8}$$

$$\approx \sigma^2_O \sigma^2_{W_{1,2}}, \tag{9}$$

where in the first line we have made the Gaussian approximation, and in the second line we have assumed that the fluctuations are much larger than the signal $\langle OW_{1,2} \rangle_c$. Thus, in the following sections we will analyse the variance of individual subdiagrams $W_{1,2}$ in order to gain a rough insight into the fluctuations of the total correction, in a similar fashion to the analysis of Ref. [10]. In that case, however, the correction to the factorization of the variance is exponentially suppressed in the separation between the vertices of the subdiagrams.

3. Quark-line disconnected subdiagram W_1

We begin by noting that the hadronic part of the diagram factorizes into two traces,

$$H_1^{\mu\nu}(x, y) = T_\mu(x) T_\nu(y), \tag{10}$$

each of which, with the current defined in Eq. (3) and in the $N_f = 2 + 1$ theory with iso-spin symmetry, is the difference of the light- and strange-quark propagators

$$T_\mu(x) = \tfrac{1}{3} \operatorname{tr}\{\gamma_\mu [S_{\text{ud}}(x, x) - S_{\text{s}}(x, x)]\}. \tag{11}$$

It is convenient to rewrite this difference as a product [10]

$$S_{\text{ud}} - S_{\text{s}} = (m_{\text{s}} - m_{\text{ud}}) S_{\text{ud}} S_{\text{s}} \tag{12}$$

which makes the explicit suppression of T_μ in the SU(3)-symmetry breaking parameter $m_{\text{s}} - m_{\text{ud}}$ explicit. This additionally results in a suppression of the variance of W_1 by $(m_{\text{s}} - m_{\text{ud}})^4$. This suppression results in a cancellation of a quartic short-distance divergence in the variance of the contribution of each individual flavour to W_1, explaining this favourable flavour combination.

While the identity in Eq. (12) is easily derived for Wilson-type fermions, here we sketch that it holds exactly for the domain-wall fermion valence propagator $S_f = \tilde{D}_f^{-1}$ which (approximately) satisfies the Ginsparg-Wilson relation [11]. Recalling the definition of $\tilde{D}_f$ in terms of the 5D Wilson matrix $D_{5,f}$ (see Ref. [12] for unexplained notation)

$$\tilde{D}_f^{-1} = (\mathcal{P}^{-1} D_{5,f}^{-1} R_5 \mathcal{P})_{11}, \tag{13}$$

where the matrix indices indicate the coordinate in the fifth dimension, the result is obtained immediately from

$$\tilde{D}_{\text{ud}}^{-1} - \tilde{D}_{\text{s}}^{-1} = (m_{\text{s}} - m_{\text{ud}})(\mathcal{P} D_{5,\text{ud}}^{-1} R_5 D_{5,\text{s}}^{-1} R_5)_{11} \tag{14}$$

by noting that the following matrix projects on the physical boundary

$$(R_5)_{..} = (R_5 \mathcal{P})_{.1} (\mathcal{P}^{-1})_{1..} \tag{15}$$

L/a	T/a	m_π	$m_\pi L$	a	$N_{\rm cfg}$
24	64	340 MeV	4.9	0.12 fm	50

Table 1: The parameters of the C1 ensemble of $N_{\rm f} = 2 + 1$ Shamir domain-wall fermions used in the numerical experiments in this work, see Ref. [17] for details.

The preceding identity is easily demonstrated using the explicit representations

$$
R_5 = \begin{pmatrix} & & P^+ \\ & & \\ P^- & & \end{pmatrix}, \qquad
\mathcal{P}^{-1} = \begin{pmatrix} P_- & & & P_+ \\ P_+ & \ddots & & \\ & & \ddots & \\ & & P_+ & P_- \end{pmatrix}, \tag{16}
$$

where $P_\pm = 1 \pm \gamma_5$.

Using the identity for the difference, there are two independent estimators for the trace

$$
\Theta_\mu(x) = \tfrac{1}{3}(m_{\rm s} - m_{\rm ud}) \frac{1}{N_{\rm s}} \sum_{i=1}^{N_{\rm s}} \eta_i^\dagger(x) \gamma_\mu \{ S_{\rm ud} S_{\rm s} \eta_i \}(x), \tag{17}
$$

$$
\mathcal{T}_\mu(x) = \tfrac{1}{3}(m_{\rm s} - m_{\rm ud}) \frac{1}{N_{\rm s}} \sum_{i=1}^{N_{\rm s}} \{ \eta_i^\dagger S_{\rm s} \}(x) \gamma_\mu \{ S_{\rm ud} \eta_i \}(x), \tag{18}
$$

where the auxiliary quark fields $\eta_i(x)$ have zero mean and finite variance. The properties of both estimators were investigated in detail in Ref. [10], where it was shown that the contribution to the variance from the auxiliary fields for the second split-even estimator was in the region of a factor O(100) smaller than the first standard estimator, which translates into the same factor reduction in the cost. The split-even estimator has since been used extensively for disconnected current correlators [13, 14, 15], while in the context of the twisted-mass Wilson formulation similar one-end trick estimators have often been employed for differences of twisted-mass propagators [16].

In this work we propose an estimator for the first diagram W_1 using

$$
\mathcal{W}_1 \approx \left(a^4 \sum_x \mathcal{T}_\mu(x) \right) \left(a^4 \sum_y \mathcal{T}_\nu(y) G_{\mu\nu}(x - y) \right) \tag{19}
$$

where independent estimators are used for the two traces to avoid incurring a bias with a finite sample size. The convolution in the second parentheses can be efficiently computed using the Fast Fourier Transform (FFT). With a minor modification, an estimator using all possible unbiased combinations of samples can be written at the cost of performing O($N_{\rm s}$) FFTs. The standard estimator is obtained by replacing both occurances of $\mathcal{T}_\mu$ with Θ_μ in Eq. (19).

We performed an analysis of the variance for the standard and split-even estimators for $\mathcal{W}_1$ using the domain-wall ensemble generated by the RBC/UKQCD collaboration whose parameters are listed in Tab. 1. The photon propagator is computed in the QED$_L$ formulation [18] in the Feynman gauge. The results for the variances, which are dimensionless numbers, are shown in Fig. 2. In addition, we plot the variance for the contribution of a single flavour $\mathcal{W}_1^{\rm u}$ using the
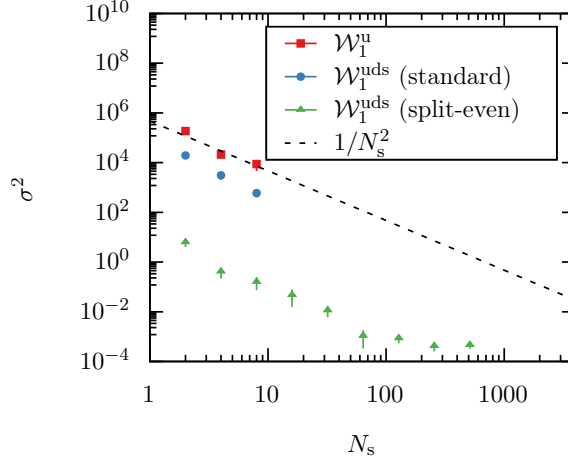
Figure 2: Left: Comparison of the variance versus the number of sources for the W_1 quark-line disconnected diagram, using a single flavour (red squares), the standard estimator for u, d, s flavours (blue circles) and the split-even estimator (green triangles). The dashed line shows $1/N_\mathrm{s}^2$ scaling. In this figure, the (local) currents are not renormalized and the charge factors are not included.

standard estimators for the traces. We note that all the variances are dominated by the fluctuations of the auxiliary fields for small N_s, and in particular scale like $1/N_\mathrm{s}^2$ in that region.

As expected, the standard estimator including the light-quark and strange-quark contributions (blue circles) is suppressed with respect to the contribution of a single flavour (red squares). Furthermore, the variance of the split-even estimator (green triangles) is reduced by a factor of 10^4 with respect to the standard one (blue circles). This reduction is commensurate with the reduction in the variance observed for the disconnected contribution to the current correlator [10], which suggests the same mechanisms are present here. For $N_\mathrm{s} \sim 100$, the variance is independent of the number of auxiliary field samples which indicates that it is dominated by the fluctuations of the gauge field. In this case no further variance reduction is possible for a fixed number of gauge configurations. Finally we note that the convolution of the second parentheses of Eq. (19) can be simply inserted sequentially in any of the diagrams of type W_3.

4. Quark-line connected subdiagram W_2

In contrast to the quark-line disconnected subdiagram, there is no cancellation in the variance in the connected subdiagram W_2 between the light and strange-quark contributions. In this case, power counting suggests that the variance diverges with the lattice spacing like a^{-4} as $a \to 0$ and is expected to be dominated by short-distance contributions. Translation averaging should therefore be very effective and one way to implement it is to use an all-to-all estimator [19] for the quark propagator

$$\mathcal{S}_f(x, x+r) = \frac{1}{N_\mathrm{s}} \sum_{i=1}^{N_\mathrm{s}} \{S_f \eta_i\}(x)\eta_i^\dagger(x+r), \tag{20}$$
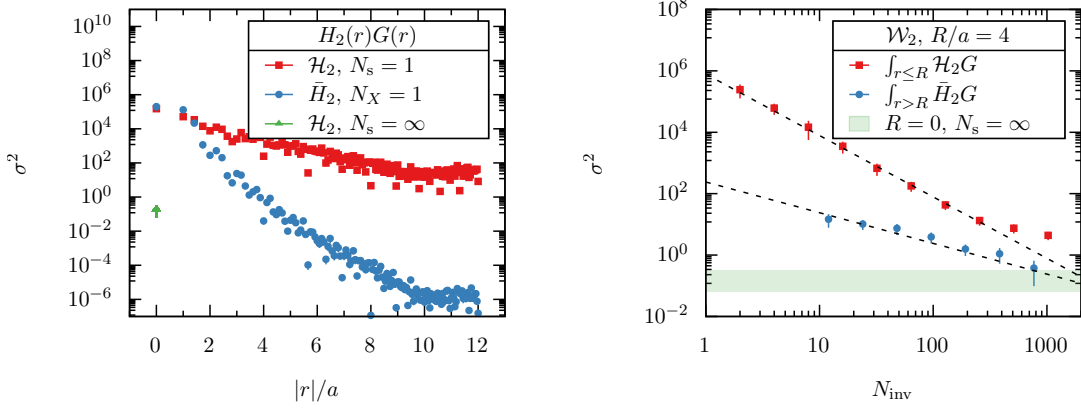
6

Figure 3: Left: the variance for the stochastic estimator (red squares) and point source estimator (blue circles) for the minimum number of inversions required, for the contribution with fixed separation between the currents $|r|$. The green triangle indicates the gauge variance for the point $r = 0$. Right: the variance for the short-distance (red squares) and long-distance (blue circles) for the choice $R/a = 4$, versus the number of inversions. The green band indicates the gauge variance for the contribution from $r = 0$ only. The dashed lines indicate the expected leading N_{inv}^{-2} and N_{inv}^{-1} scaling for the short- and long-distance components.

using independent fields for each propagator in the trace

$$\mathcal{H}_2^{\mu\nu}(r) = a^4 \sum_x \sum_f Q_f^2 \operatorname{tr}\{\gamma_\mu \mathcal{S}_f(x, x+r)\gamma_\nu \mathcal{S}_f(x+r, x)\}. \tag{21}$$

As written, the estimator is feasible to compute for a small number of separations r between the vertices and, although it introduces a (mild) signal-to-noise ratio problem at large r, should be efficient at small $|r| \leq R$ given the leading extra contribution vanishes like N_s^{-2}, c.f. Sec. 3.

For the remainder $|r| > R$, we propose using N_X randomly selected point sources X_n [20]

$$\bar{H}_2^{\mu\nu}(r) = \frac{L^3 T}{N_X} \sum_{n=1}^{N_X} H_2^{\mu\nu}(X_n, X_n + r) \tag{22}$$

so that the total is split between short- and long-distance contributions

$$\mathcal{W}_2 = a^4 \sum_{|r| \leq R} \mathcal{H}_2(r) G_{\mu\nu}(r) + a^4 \sum_{r > R} \bar{H}_2^{\mu\nu}(r) G_{\mu\nu}(r), \tag{23}$$

using the efficient stochastic estimator for the noisy short-distance contribution. Ref. [21] introduced an importance sampling based on current separations for higher-point correlation functions, whereas in this case we make the separation based on the expected contributions to the variance. This approach avoids completely factorizing the trace which would require either O(V) contractions or O(N_s^2) FFTs to include the photon line which we deemed unfeasible.

In Fig. 3 (left) we illustrate the variance of each of the terms in Eq. (23) for the sum over a fixed separation $|r|$ between the currents, for the case $N_s = N_X = 1$. As expected, the variance from the contribution around $|r| \sim 0$ dominates both the stochastic (red squares) and point source estimator (blue circles), and we observe the mild signal-to-noise ratio problem in the stochastic

estimator. The green triangle denotes the gauge variance for the case $r = 0$, which is approximately suppressed by $(L^3 T)/a^4$ compared to $N_X = 1$ indicating translation averaging is very effective for the short-distance contribution. In the right-hand panel, we see variance of the short- and long-distance contributions with the choice $R/a = 4$ as a function of the number of inversions (where $N_X = 1$ corresponds to 12 inversions). The variance is dominated by the short-distance contribution (red squares) which however scales favourably like N_{inv}^{-2}, while the long-distance contribution (blue circles) which scales only like N_{inv}^{-1} is much suppressed. Deviations from the former scaling indicate that the gauge variance may be reached with just $N_{\text{inv}} \sim 1000$, which although is larger than required for W_1 is still achievable with modern computational resources, and universal for all observables.

5. Conclusions

In this work we have examined the Wick contractions which arise due to the charge of the sea quarks in the RM123 method. Such diagrams contribute, in principle, even to observables constructed from neutral fields and are therefore ubiquitous in the computation of iso-spin breaking corrections. We have proposed stochastic estimators for the quark lines in such diagrams which completely avoids the need to sample the Maxwell action stochastically, thus eliminating one additional source of variance. As for the case of disconnected contributions to current correlators, we have shown it is beneficial to consider certain flavour combinations which have greatly suppressed fluctuations. We have shown that the split-even estimators generalize also to domain-wall fermions and perform well compared with naïve estimators. Thus the frequency-splitting strategy of Ref. [10] should generalize appropriately for this fermion formulation. In the second topology, however, there is no cancellation of the short-distance effects in the variance by considering multiple flavours. In this case, we propose decomposing the diagram into a short-distance part to be estimated stochastically and a long-distance part estimated using position-space sampling. The variance is reduced sufficiently so that the gauge variance can be reached with a reasonable computational cost. Given their short-distance nature, these estimators should also succeed with smaller quark masses, and furthermore as the diagrams are universal to all iso-spin breaking corrections we anticipate that these simple decompositions ought to be beneficial in large-scale simulations. In particular we are developing these methods for refinements of our computations of iso-spin breaking corrections within the RBC/UKQCD collaboration, for example to meson (leptonic) decay rates [22, 23].

References

[1] T. Aoyama et al. In: *Phys. Rept.* 887 (2020), pp. 1–166. arXiv: 2006.04822 [hep-ph].

[2] Y. Aoki et al. In: *Eur. Phys. J. C* 82.10 (2022), p. 869. arXiv: 2111.09849 [hep-lat].

[3] S. Aoki et al. In: *Phys. Rev. D* 86 (2012), p. 034507. arXiv: 1205.2961 [hep-lat].

[4] T. Ishikawa et al. In: *Phys. Rev. Lett.* 109 (7 Aug. 2012), p. 072002.

[5] R. Horsley et al. In: *J. Phys. G* 46 (2019), p. 115004. arXiv: 1904.02304 [hep-lat].

[6] L. Bushnaq et al. In: (Sept. 2022). arXiv: 2209.13183 [hep-lat].

[7] S. Borsanyi et al. In: *Nature* 593.7857 (2021), pp. 51–55. arXiv: 2002.12347 [hep-lat].

[8] G. M. de Divitiis et al. In: *JHEP* 04 (2012), p. 124. arXiv: 1110.6294 [hep-lat].

[9] G. M. de Divitiis et al. In: *Phys. Rev. D* 87.11 (2013), p. 114505. arXiv: 1303.4896 [hep-lat].

[10] L. Giusti et al. In: *Eur. Phys. J. C* 79.7 (2019), p. 586. arXiv: 1903.10447 [hep-lat].

[11] S. Capitani et al. In: *Nucl. Phys. B* 593 (2001), pp. 183–228. arXiv: hep-lat/0007004.

[12] T. Blum et al. In: *Phys. Rev. D* 93.7 (2016), p. 074505. arXiv: 1411.7017 [hep-lat].

[13] T. San José et al. In: *JHEP* 08 (2022), p. 220. arXiv: 2203.08676 [hep-lat].

[14] E.-H. Chao et al. In: *Eur. Phys. J. C* 81.7 (2021), p. 651. arXiv: 2104.02632 [hep-lat].

[15] M. Salg et al. In: *39th International Symposium on Lattice Field Theory*. Nov. 2022. arXiv: 2211.17049 [hep-lat].

[16] P. Boucaud et al. In: *Comput. Phys. Commun.* 179 (2008), pp. 695–715. arXiv: 0803.0224 [hep-lat].

[17] C. Allton et al. In: *Phys. Rev. D* 78 (2008), p. 114509. arXiv: 0804.0473 [hep-lat].

[18] M. Hayakawa and S. Uno. In: *Prog. Theor. Phys.* 120 (2008), pp. 413–441. arXiv: 0804.2044 [hep-ph].

[19] G. M. de Divitiis et al. In: *Phys. Lett. B* 382 (1996), pp. 393–397. arXiv: hep-lat/9603020.

[20] Y. Li et al. In: *Phys. Rev. D* 103.1 (2021), p. 014514. arXiv: 2009.01029 [hep-lat].

[21] T. Blum et al. In: *Phys. Rev. Lett.* 124.13 (2020), p. 132002. arXiv: 1911.08123 [hep-lat].

[22] P. Boyle et al. In: (Nov. 2022). arXiv: 2211.12865 [hep-lat].

[23] P. Boyle et al. In: *39th International Symposium on Lattice Field Theory*. Dec. 2022. arXiv: 2212.04709 [hep-lat].

[24] P. A. Boyle et al. In: *PoS* LATTICE2015 (2016), p. 023.